X-ray Physics - AN10

James R. McMurray
Demonstrator: Alan Usher
(Dated: December 2, 2010)

X-rays were produced by bombarding molybdenum and tungsten anodes with electrons to produce a continuous Bremsstrahlung distribution of X-rays and characteristic peaks from stimulated photon emission. The X-rays were then used to calculate the lattice constant, a_0, of a sodium chloride crystal, and the spectrum of the X-rays was analysed to produce an experimental estimate for Planck's constant. The lattice spacing was found to be 565 ± 5 pm, which is consistent with the accepted value of 564.02 pm. The experimental value of Planck's constant was found to be $6.6(0.1) \times 10^{-34}$ Js, which is consistent with the accepted value of 6.63×10^{-34} Js.

INTRODUCTION

In this investigation X-ray sources were used to examine the structure of a sodium chloride crystal from the diffraction pattern, and the edge length of the conventional cubic unit cell, a_0, was determined. The spectrum of X-rays produced from the source was also analysed and an experimental value for Planck's constant was calculated.

X-rays were first produced and detected by Wilhelm Röntgen in 1895 using the same principle of accelerating electrons towards a metal target that was used in this experiment[1]. However, Röntgen used a Crookes tube to produce the electrons for bombardment, and so, due to the design of the Crookes tube, was unable to vary the potential and current independently[2]. In 1913, William Coolidge invented the Coolidge tube, which produces electrons by thermionic emission from a heated filament. This method allows the potential and the current to be changed independently[2], and it was this method that was used in this experiment.

In 1912, von Laue was the first to propose that X-rays could be diffracted by crystals and carried out an experiment to demonstrate his idea[3]. These two discoveries led to the creation of the field of X-ray crystallography, in which the structure of crystals is examined by their diffraction of X-rays. In this experiment the structure of a sodium chloride crystal is analysed by the same methods.

THEORY

X-ray Production

The X-rays were produced by accelerating electrons towards a molybdenum or tungsten anode, whereby the electrons underwent rapid deceleration, creating X-rays in Bremsstrahlung (braking radiation) and also by stimulating photon emission in the atoms of the anode.

The electrons were produced by thermionic emission from a heated filament in the X-ray tube. Note that the supply voltage to the filament and the accelerating voltage are separate supplies.

Bremsstrahlung

Bremsstrahlung (braking radiation) is the radiation produced by the acceleration of a charged particle when it is deflected by another charged particle. In this experiment it is produced due to the rapid deceleration of the electrons as they collide with the anode atoms. This radiation is produced because an accelerating charge emits radiation (this is the same phenomenon that produces cyclotron radiation), this can be shown from the wave-like solutions to Maxwell's equations, however the derivation is too long to be reproduced in this report. See [4] for the full derivation.

Bremsstrahlung is a continuous spectrum of radiation, since the electrons undergo different decelerations depending on how directly they strike the anode atoms. It has a sharp cut-off at low wavelengths, this cut-off wavelength is dependent on the energy of the incoming electrons. It can be calculated by using the Planck relation and the kinetic energy of the accelerated electrons[1]:

$$E_{photon_{max}} = hf_{max} = \frac{hc}{\lambda_{minimum}} \tag{1}$$

$$E_k = eV \tag{2}$$

$$\therefore \ \frac{hc}{\lambda_{minimum}} = eV \tag{3}$$

$$\therefore \ \lambda_{minimum} = \frac{hc}{eV} \tag{4}$$

Where V is the potential of the electric field used to accelerate the electrons, h is Planck's constant, c is the speed of light, e is the charge of the electrons and $\lambda_{minimum}$ is the minimum wavelength of the emitted X-rays.

Figure 1 is an example plot of a Bremsstrahlung distribution, without any peaks from stimulated emission. Note that increasing the accelerating potential decreases the minimum wavelength and the peak wavelength[5].

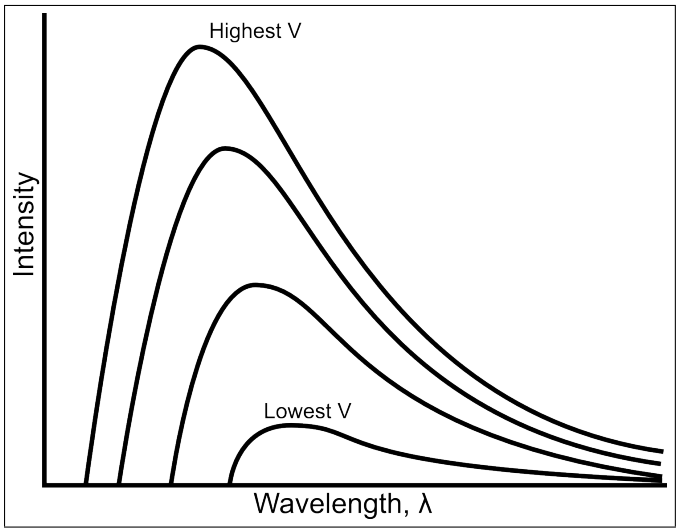

FIG. 1: An example plot of a hypothetical Bremsstrahlung distribution without interference from other sources. The different lines demonstrate the effect of varying the accelerating potential, V.

Stimulated Emission

The collision of the accelerated electrons with the anode atoms also produces X-ray photons by stimulated emission from the anode atoms. This is caused by the the incoming electrons ejecting core electrons from the anode atoms, the outer electrons then fall down a certain number of energy levels to fill this vacancy, and photons are emitted with the energy of the difference between the energy levels (such that energy is conserved). This phenomenon is a consequence of the quantisation of energy levels first proposed by Max Planck in 1900.

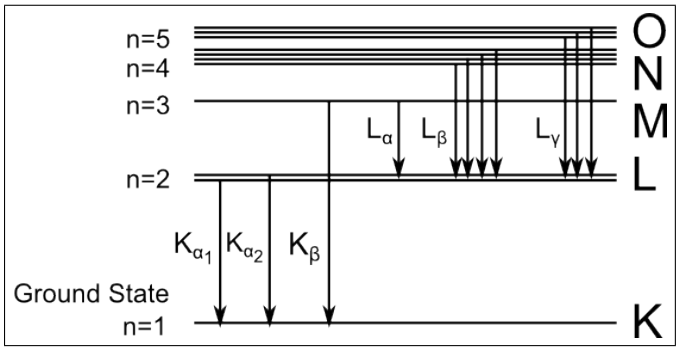

FIG. 2: A diagram showing the relevant changes in energy levels that produce X-ray photons. Note the energy levels above the ground state ($n \geq 2$) are split in to multiple energy levels due to the differences in energy between the different orbitals.

For the molybdenum anode, the X-ray photons are produced by electrons in the 2nd and 3rd energy shells (L and M) dropping to the ground state (the innermost shell, K), as shown in Figure 2. The $L \rightarrow K$ transition produces photons with a wavelength of 71.08 pm, this is the K_α line. The $M \rightarrow K$ transition produces photons of wavelength 63.09 pm, this is the K_β line[6]. For the tungsten anode the X-rays are produced by the L_α, L_β and L_γ transitions labelled in Figure 2, the wavelengths for X-rays produced by the L_α and L_β transitions are 148 pm and 128 pm respectively[6]. The wavelength of the X-rays produced by the L_γ transition is to be determined, the accepted value is 109.87 pm[7]. Many other transitions also occur, in both anodes, however these transitions do not result in the production of X-ray photons and so will not be detected in the experiment.

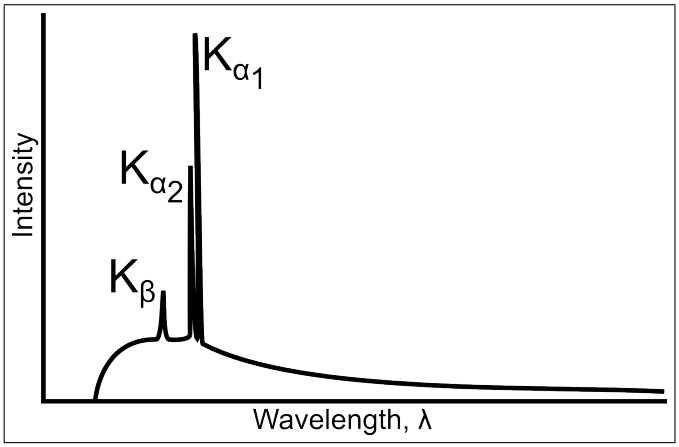

FIG. 3: An example plot of the specific wavelength peaks from stimulated emission and their relative intensities. The continuous spectra is produced from the Bremsstrahlung radiation described previously.

Note that the energy levels above the ground state are actually split in to multiple levels due to the differences in energy between the orbitals. This results in multiple, close peaks that make up the K_α and K_β lines, however these peaks may be too close together to be resolved with the apparatus (especially the split K_β peaks as the relative energy difference is very small)[8].

The expected peaks in intensity are shown in Figure 3. The average of the intensity of the K_α peaks should be approximately 5 to 10 times the intensity of the K_β peak. Meanwhile the K_{α_1} peak should be approximately twice the intensity of the K_{α_2} peak[8].

Other effects

In the production of the X-rays, other physical phenomena are also observed such as the photoelectric effect and the Auger effect.

In the photoelectric effect, electrons are emitted from an atom due to the absorption of a photon. It occurs in this experiment when an emitted X-ray photon is absorbed by a molybdenum atom, and the increased energy causes the ejection of an electron from the atom (this

emitted electron is termed a photoelectron).

The transition of an electron from an outer shell to a vacancy in the core causes the release of energy, some of which is transferred to other electrons (and the production of photons). The Auger effect occurs when this transferred energy is enough to cause a second electron to be emitted from the atom. This second electron is termed an Auger electron[9]. Note that this can cause a chain of Auger electrons to be produced, as the ejection of the Auger electron leaves a vacancy in the core shell which may then cause another Auger electron to be produced as the vacancy is filled. This can continue until the energy produced by the energy level transition is less than the ionisation energy of the core electrons.

X-ray Diffraction

The periodicity of crystals causes them to strongly diffract light when the wavelength is of the same order as the distance between the planes of atoms in the crystal. Because the distance between neighbouring atoms is very small, crystal diffraction could not be observed until the discovery of X-rays.

As the X-rays intercept the planes of the crystal, they are scattered by the electrons in multiple directions. This leads to interference between the scattered rays which results in the Bragg condition.

Crystal structure

Crystals consist of planes of regularly arranged atoms. Sodium chloride forms a crystal with a Face-Centred Cubic (FCC) lattice and a two-atom basis as shown in Figure 4.

Note that the basis is only two atom as the ions on the edges and vertices are shared with neighbouring cells. The total number of lattice points per cell is 4, and so there are 8 atoms per cell due to the two-atom basis.

The smallest unit cell possible is rhombohedral, with an ion at $(0,0,0)$ and another ion at $\frac{1}{2}(\vec{a_1},\vec{a_2},\vec{a_3})$, as shown in Figure 5. Note that two of these unit cells are necessary to fully describe the crystal structure, one with a sodium ion at $(0,0,0)$ (and so a chloride ion at $\frac{1}{2}(\vec{a_1},\vec{a_2},\vec{a_3})$) and one with the ion positions swapped. [10].

Note that due to the two-atom basis, the atomic spacing, d, is half the length of the conventional cell cube edge, a_0.

$$d = \frac{a_0}{2} \tag{5}$$

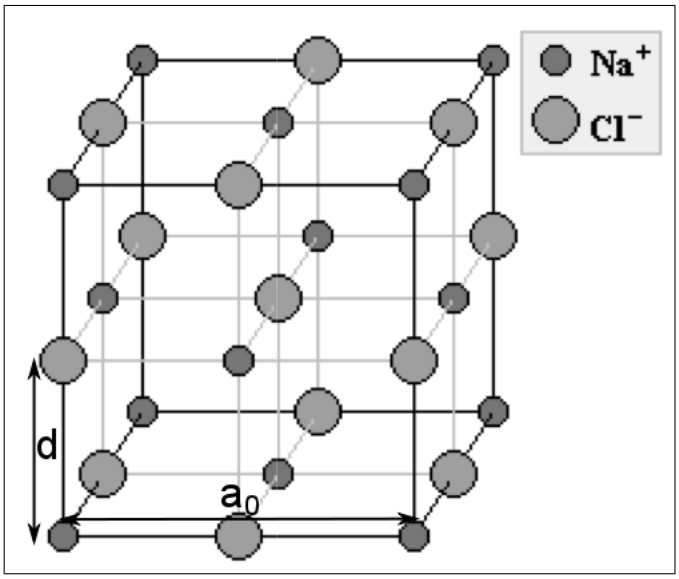

FIG. 4: A diagram of the structure of an NaCl crystal. In this diagram, the sodium ions are drawn on lattice points. Modified, originally from [10].

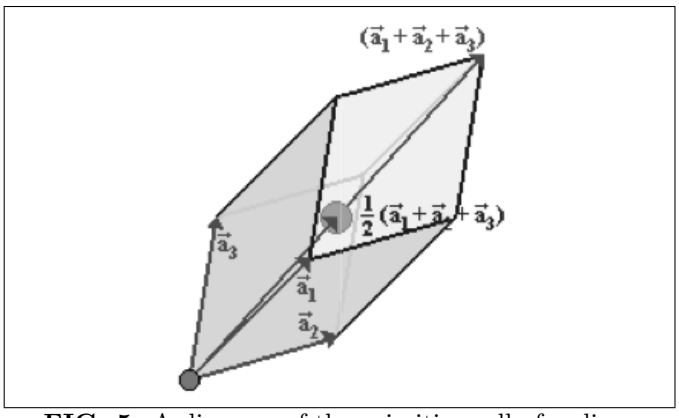

FIG. 5: A diagram of the primitive cell of sodium chloride. Note that two such primitive cells are necessary to fully describe the crystal structure, one with a sodium ion at the origin and a chloride ion in the centre and another with the positions swapped. Taken from [10].

Bragg diffraction

In most directions the scattered rays cancel each other out through destructive interference, however in a few directions the rays interfere constructively.

The Bragg condition provides the condition for this constructive interference to occur. It arises because each layer of atoms only partially reflects the incoming X-rays. This produces interference in the scattered rays as there is a path difference dependent on the number of planes the ray penetrated before reflection, and so an associated phase difference, as shown in Figure 6.

The Bragg condition is derived as follows:

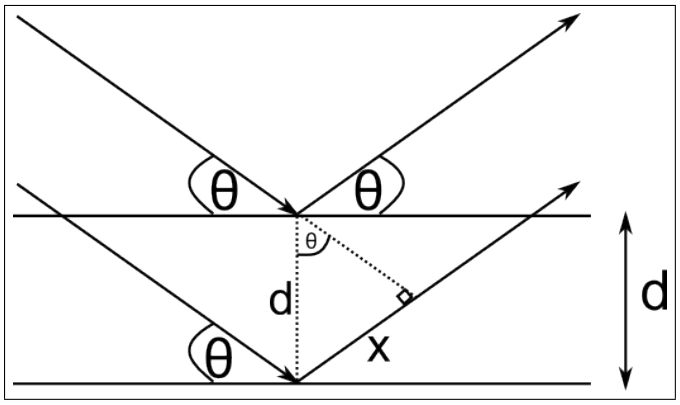

FIG. 6: A diagram showing the reflection of X-rays from the surface of a crystal. Note the path difference, x, which is created between reflected rays and leads to interference and the Bragg condition.

From Figure 6:

$$\text{Path difference } = 2x = 2dsin(\theta) \tag{6}$$

For the interference to be constructive, the path difference must be an integer multiple of the wavelength:

$$\text{Path difference}, 2x = n\lambda \tag{7}$$

Combining equations (6) and (7):

$$n\lambda = 2dsin(\theta) \tag{8}$$

Where n is the order of reflection, d is the distance between adjacent planes of the crystal and θ is the angle that the X-rays are incident on the crystal surface. This is the Bragg condition, when it is satisfied constructive interference will be detected. Note that the relationship is very sensitive, as the effects of each of the layers fo atoms add up, this means that think peaks are produced when the Bragg condition is satisfied, whilst the destructive interference is dominant elsewhere.

The Reciprocal Lattice

The reciprocal lattice is a mathematical construct, derived from the real space lattice, which describes which sets of planes in the real space lattice will result in Bragg diffraction.

The sets of planes in the real space lattice are defined by Miller indices, (hkl) which give the reciprocals of the fractional co-ordinates where the planes intercept the co-ordinate axes. In the reciprocal lattice, the Miller indices of the reflecting planes give the fractional co-ordinates of the reciprocal lattice points.

The reciprocal lattice of the FCC real space lattice is a BCC lattice, and so the Miller indices of the reflecting planes (the fractional co-ordinates of the reciprocal lattice points) are subject to the constraint that h, k, l must be all even or all odd.

Note that in this experiment, due to the geometry maintained by the coupled mode of the goniometer, the distance between the reflecting planes is always $\frac{a}{2}$ as shown in Figure 4. This means that the reflecting planes are subject to an additional constraint as substituting Equation (5) in to the Bragg condition (Equation (8)) obtains:

$$a = \frac{n\lambda}{sin(\theta)} \tag{9}$$

But from the definition of the cubic reciprocal lattice:

$$d = \frac{a}{\sqrt{h^2 + k^2 + l^2}} \tag{10}$$

Substituting this in to the Bragg condition, taking n in to the h, k and l variables, obtains:

$$a = \frac{\lambda\sqrt{h^2 + k^2 + l^2}}{2sin(\theta)} \tag{11}$$

Equating equations (9) and (11) yields:

$$n^2 = \frac{h^2 + k^2 + l^2}{4} \tag{12}$$

Where n, h, k and l are all integers. This additional condition means that only reflections from the (200), (400) and (600) sets of planes are observed, as the first-order, second-order and third-order peaks respectively.

X-ray detection

The X-rays are detected by the Geiger-Müller (GM) tube. The GM tube contains an inert gas which is ionised by the incoming X-ray photons, these ions are then accelerated by the potential in the tube, producing a current when they reach the cathode. Note that the current is not proportional to the number of X-ray photons in a traditional GM tube, since the acceleration of the ions is rapid enough such that resultant collisions can produce more ions, this is useful since it means that faint radiation can be detected, however it means X-rays arriving in a very rapid succession will be detected as one. To overcome this problem, the counters are rapidly quenched after detection, usually by the addition of organic molecules to the inert gas mixture, which quench the tube since they dissociate in to smaller, neutral molecules on ionisation rather than producing a current[3].

METHOD

The X-rays were produced in a Coolidge tube (shown in Figure 7), an X-ray collimator was then used to pro-

duce a narrow beam of X-rays from the resultant emission. This fine beam was then aimed at the sodium chloride crystal, at an angle of θ to the crystal's surface.

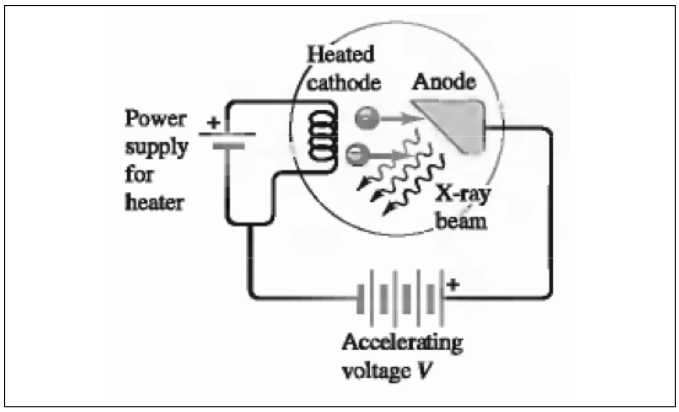

FIG. 7: A diagram of a Coolidge tube, the cooling elements have been omitted. Note that the accelerating voltage and the supply voltage to heat the cathode are separate supplies. Taken from [1].

Note that the collimator does not act as a lens (as collimators for visible light do), as the short wavelengths mean this is not possible, instead the collimator consists of X-ray absorptive material, with small gaps such that only the X-rays which are travelling perpendicular to the collimator can pass through. Note that this method is not perfect as the gaps must be large enough to prevent significant diffraction, and so there may still be some difference in direction in the resultant X-rays[3].

The apparatus is essentially a Bragg spectrometer, a diagram of the apparatus, when set up, is shown in Figure 8.

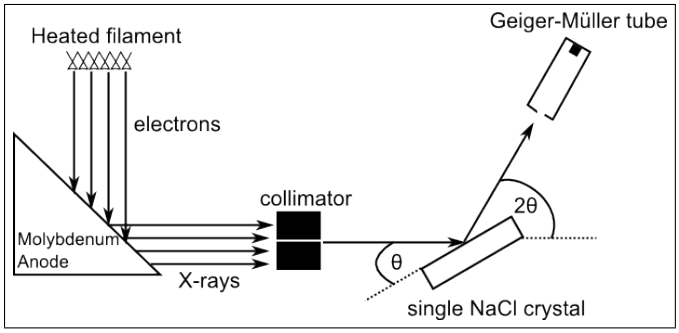

FIG. 8: A diagram of the apparatus when set up. Note that the X-rays are produced and scattered in many directions, however only the relevant ones are shown.

The Geiger-Müller tube and target crystal are both rotated, by a goniometer, such that the angle θ is changed, meanwhile the ratio of θ to 2θ is maintained. Note that the apparatus must be set up correctly so that when the goniometer angle is zero, the apparatus is arranged as in Figure 8, otherwise the ratio of angles will not be accurately maintained during the rotation.

Determining the atomic spacing in a sodium chloride crystal

In this part of the experiment, the atomic spacing, d, between adjacent planes of atoms in the sodium chloride crystal was determined. The edge length of the conventional cubic cell, a_0, can also be calculated since this is simply twice the atomic distance.

Re-arranging the Bragg condition (Equation (8)) obtains:

$$d = \frac{n\lambda}{2sin(\theta)} \tag{13}$$

Where the variables are the same as defined previously.

Then by noting when constructive interference is observed (and the characteristic peaks are detected), the atomic spacing may be determined, since it must be constant.

The Bremsstrahlung X-rays cannot be used to determine the lattice spacing since they produce a continuous distribution and so the wavelengths are not known.

The current accepted value of the lattice spacing (the length of the edge of the lattice cube) for sodium chloride is 5.640×10^{-10} m[10], and so an atomic spacing of 2.82×10^{-10} m.

The X-ray tube voltage was set at 35 kV and the emission current was set to 1 mA. The measuring time per angular step was 10 seconds, with a total of 300 measurements, the automated apparatus took 50 minutes to take the results.

Handling experimental uncertainty

In this part of the experiment a large amount of data was produced (300 results for each anode), however most of these measurements cannot be used in the calculation of a_0, since the wavelengths are not known, and so only the peaks of known wavelength can be used.

The experimental error in the calculated lattice spacing can be approximated by taking the mean value of the results to be the true lattice spacing, and using the standard error in the mean as the error in this value. The standard error is used rather than just the standard deviation, since the standard deviation provides an estimate for the error in a single result, whilst the standard error provides an estimate for the error in the mean average of the results.

$$SE_{\bar{x}} = \frac{s}{\sqrt{n}} \tag{14}$$

The calculation of the standard error in the mean is shown in Equation (14). Where $SE_{\bar{x}}$ is the standard error in the mean, s is the standard deviation in the data

sample (the calculation of which is shown in Equation (15)) , and n is the number of observations in the sample.

$$s = \sqrt{\frac{1}{N-1}\sum_{i=1}^{N}(x_i - \bar{x})^2} \tag{15}$$

Where s is the standard deviation of the sample, N is the total number of results, x_i is the ith result of the set, and $\bar{x}$ is the mean of the data. Note the use of Bessel's correction ($N-1$ in the denominator instead of N) to ensure accuracy with the small number of results.

Note that the standard error can be halved by taking four times as many measurements, and so the experimental uncertainty can be reduced greatly by taking many more measurements.

However, this statistical method only takes in to account the random error in the measurements, and not systematic error due to the inherent uncertainty in the angular steps of the goniometer. Using the partial derivative method of error analysis takes account of this systematic error. Assuming there is no error in n and the accepted values of λ for the stimulated emission peaks, then the only systematic error present is in θ, and so the equation for the error in the lattice spacing a_0 is as shown in Equation (16).

$$\Delta a_0 = \left|\frac{\partial a_0}{\partial \theta}\right| \Delta\theta \tag{16}$$

Differentiating and substituting the Bragg equation (Equation (8)) obtains Equation (17).

$$\Delta a_0 = \left|\frac{n\lambda cos(\theta)}{sin^2(\theta)}\right| \Delta\theta \tag{17}$$

Where Δa_0 is the experimental uncertainty in the lattice constant and $\Delta\theta$ is the experimental uncertainty in the scattering angle (note that this must be used in radians), which is taken to be $0.1°$ as this was the minimum step size of the goniometer.

Measuring the X-ray spectrum of the X-ray tube

The Bragg condition (Equation (8)) shows that different wavelengths are diffracted at different angles from the surface of the crystal. By combining the Bragg condition with Planck's relation, an equation relating the energy of the incident rays, E, with the angle of reflection, θ, is obtained:

$$E = hf = \frac{hc}{\lambda} \tag{18}$$

$$\lambda = \frac{2dsin(\theta)}{n} \tag{19}$$

Substituting for λ:

$$\frac{hc}{E} = \frac{2dsin(\theta)}{n} \tag{20}$$

$$E = \frac{nhc}{2dsin(\theta)} \tag{21}$$

The relations for wavelength, λ and X-ray photon energy, E, with θ can be used to observe how the wavelength and energy distributions vary when the emission current and accelerating voltage are changed.

Note that we can assume $n = 1$ for this data, as the effect of the second order reflections on the Bremsstrahlung radiation will be negligible and the angle range is not large enough to detect second reflections from the peaks.

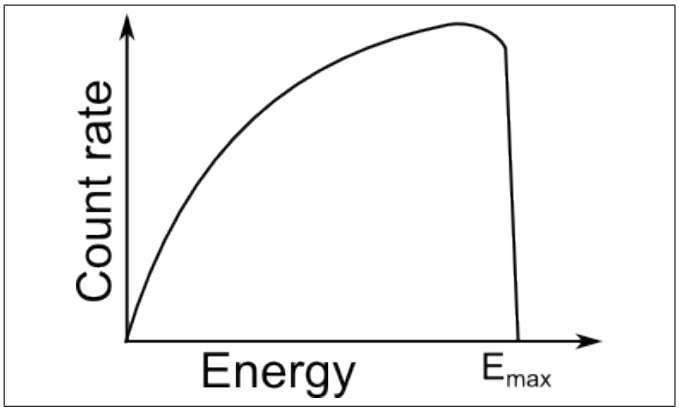

FIG. 9: An example plot of energy against count rate. E_{max} is the maximum possible energy, where all the kinetic energy of the incoming electrons has been converted in to photon energy.

An example plot showing the expected shape of the data is shown in Figure 9. There is a sharp cut-off at the maximum possible energy, where all the kinetic energy of the incoming electrons has been converted to photon energy, in this case the energy is given by Equation (2).

In this part of the experiment only the molybdenum anode was used.

Changing the accelerating voltage

In this part of the experiment, the X-ray tube voltage was varied from 15.0 kV to 35.0 kV, in steps of 2.5 kV, and a set of measurements was taken at each step. The emission current was kept constant at 1.00 mA, and θ was varied from $2.5°$ to $12.5°$ in steps of $0.1°$ with a measurement time of 10 seconds as previously. The coupled rotation is used as in the first part of the experiment to maintain the $\theta : 2\theta$ ratio shown in Figure 8.

From Equation (4), it is expected that the minimum wavelength of the continuous Bremsstrahlung radiation will decrease as the accelerating voltage is increased.

The K_α and K_β peaks will not be present for low voltages, as the collision of any particular electron will not provide enough energy to the molybdenum atoms to eject core electrons and produce the relevant electron transitions.

The position of the peaks should not change with varying voltage, as the peaks are produced by specific energy level transitions which have characteristic wavelengths.

The intensity of the peaks will increase with increasing voltage, because, as the voltage is increased, the electrons will have enough kinetic energy to cause the emission of multiple X-ray photons.

Changing the emission current

In this part of the experiment, the X-ray tube voltage was kept constant at 35 kV, the emission current is initially set at 0.40 mA, and was increased in steps of 0.20 mA up to 1.00 mA. The sets of measurements are taken using the same settings as for varying the voltage.

As the current is increased, the intensity of the peaks and the Bremsstrahlung radiation should increase, as there are more electrons with the required energy for stimulated emission, and with the entire range of energies for the Bremsstrahlung radiation.

Note that in both cases (varying the emission current and varying the voltage) there is a minimum wavelength beyond which no X-rays are emitted. This is because there is a minimum wavelength for the Bremsstrahlung radiation shown in Equation (4).

Determining a value for Planck's constant

Equation (4) shows that:

$$\lambda_{min} = \frac{hc}{e}\frac{1}{V} \tag{22}$$

And so by plotting a graph of λ_{min} against $\frac{1}{V}$, a straight line graph passing through the origin should be obtained. A value for Planck's constant, h, can then be calculated:

$$\text{gradient} = \frac{hc}{e} \tag{23}$$

$$\therefore\ h = \frac{\text{gradient} \times e}{c} \tag{24}$$

Handling experimental uncertainties

An estimate for the fractional error, E_{frac}, of the gradient of the straight line fit for the graph of λ_{min} against $\frac{1}{V}$ can be calculated using equation (25).

$$E_{\text{frac}} = \frac{\sum_{i=1}^{N} \frac{|y_i - y_{\text{fit}}|}{y_{\text{fit}}}}{N} \tag{25}$$

Where y_i is the ith result, y_{fit} is the value on the fit corresponding to this result and N is the total number of results.

Assuming there is negligible error in the speed of light c, and the charge of the electron e (as these are both well studied constants), then the fractional error in the gradient is the same as the fractional error in the experimental value of Planck's constant.

However, this statistical method does not account for systematic errors such as the inherent error in the minimum wavelength due to the difficulty of judgement and the error in the tube voltage due to the uncertainty in the power supply. The partial derivative method of uncertainty analysis will take account of the systematic error.

Rearranging Equation (4) for h obtains Equation (26).

$$h = \frac{\lambda_{\text{min}} eV}{c} \tag{26}$$

Assuming there is no error in the values of e and c, applying the partial derivative method obtains the following equation for the uncertainty in h.

$$\Delta h = \sqrt{\left(\frac{eV}{c}\Delta\lambda_{\text{min}}\right)^2 + \left(\frac{\lambda_{\text{min}} e}{c}\Delta V\right)^2} \tag{27}$$

Where Δh is the uncertainty in the experimental value of Planck's constant, e is the charge of an electron, c is the speed of light in a vacuum, $\Delta\lambda_{\text{min}}$ is the uncertainty in the minimum wavelength (estimated to be 1 pm) and ΔV is the uncertainty in the tube voltage, which is estimated to be 0.1 kV as this was the smallest step available on the X-ray tube.

Safety

X-rays have enough energy to ionize atoms they collide with and so present a danger to human health (as the ionisation of molecules in cells can cause cancer growth). The apparatus is shielded to protect the operators from the X-rays at all times, however care must be taken to ensure the interlocking mechanism is operational, and so if the door is open, the X-ray production will halt.

ANALYSIS

Determining the lattice constant of NaCl

Plots of the data for the molybdenum and tungsten anodes are shown in Figures 10 and 11 in Appendix I respectively.

The relevant peak information is shown in Table I.

TABLE I. The peak information for the molybdenum and tungsten anodes

n	Peak type	λ, pm	$sin(\theta)$	a_0, pm
1	K_β	63.09	1.1147×10^{-1}	566.00
1	K_α	71.08	1.2533×10^{-1}	567.14
2	K_β	63.09	2.2325×10^{-1}	565.20
2	K_α	71.08	2.5207×10^{-1}	563.97
3	K_β	63.09	3.3545×10^{-1}	564.23
3	K_α	71.08	3.7784×10^{-1}	564.37
1	L_β	128.00	2.2665×10^{-1}	564.75
1	L_α	148.00	2.6219×10^{-1}	564.48

Due to the peak splitting in the second order peaks for the tungsten anode, these peaks were not used in calculating a value for the lattice constant. The peak due to L_γ is also not used for this calculation as the wavelength of this transition was not provided and is to be calculated.

Using this data, the mean value for the lattice constant is 565.02 pm. The random error in this value (calculated using equations (14) and (15)) is ± 0.38 pm, while the systematic error (calculated using Equation (17)) is $\pm 4.7pm$. This gives the experimental value of the lattice constant as 565 ± 5 pm (as the greatest error takes precedence, and the errors are used to one significant figure), this is consistent with the accepted value of 564.02 pm.

Table II shows the accepted wavelengths of the energy transitions for the tungsten anode, which were used to label the split peaks in Figure 11.

TABLE II. The accepted wavelengths of the tungsten energy transitions. Selected from [7].

Transition	λ, pm
L_{α_1}	147.67
L_{β_1}	128.20
L_{β_2}	124.49
L_{β_3}	126.27
L_{β_4}	130.15
L_{γ_1}	109.87
L_{γ_2}	148.75
L_{γ_3}	106.19

Calculating the wavelength of the L_γ peak

From the data, the wavelength of the L_γ peak can be calculated. The first order L_γ peak was observed at a $sin(\theta)$ value of 1.9595×10^{-1}. Re-arranging the Bragg condition (Equation (8)) for λ obtains and substituting the accepted value of a_0 (564.02 pm):

$$\lambda = \frac{a_0 sin(\theta)}{n} \tag{28}$$

This obtains a value of the wavelength as 110.5 pm. The accepted value for the wavelength of the L_γ peak is 109.9 pm[7]. This is only a difference of 0.5% from the accepted value.

Investigating the X-ray spectrum of the X-ray tube

This part of the experiment used only the molybdenum anode, the relevant graphs are in Appendix II, only the plots of the data at the extreme ends of the voltage and current are included, and the tube voltage at which the peaks are first visible. Note that there are significant variations in the count rate between the graphs.

The peak intensity increases with increasing tube voltage, this is because the incoming electrons will have enough energy to cause the emission of multiple x-ray photons. The intensity of the Bremsstrahlung radiation also increases with increasing voltage, as the electrons will undergo greater deceleration on collision with the anode atoms, causing the emission of a greater number of photons. Increasing the tube voltage also shifts the entire distribution to higher energies.

The position of the peaks does not change with varying voltage, as the peaks are produced by specific energy level transitions which have characteristic wavelengths.

For increasing current the intensity of the whole distribution increases, but the energies and shape of the distribution are unchanged.

The stimulated emission peaks are first observed at a tube voltage of 25 kV, as shown in Figure 15. They are absent for tube voltages of 15kV, 17.5kV, 20kV and 22.5 kV. The energies of the K_α and K_β peaks are 17.5 keV and 19.7 keV (calculated using Equation (18)). The peaks are absent for tube voltages of 15kV and 17.5kV because the incoming electrons do not have enough energy to stimulate the emission of the X-ray photons (even if they collide head-on). The peaks are not observed at tube voltages of 20kV and 22.5kV (despite these being greater than the energy of the transitions) because the small increase over the required energy means that very few electrons will collide directly enough to transfer enough energy to the molybdenum atoms to produce the stimulated emission.

The minimum wavelengths for each tube voltage are shown in Table III.

TABLE III. The minimum wavelengths produced for each tube voltage

Tube Voltage, kV	Tube Voltage^{-1}, kV^{-1}	λ_{minimum}, pm
15.0	0.067	80.4
17.5	0.057	69.7
20.0	0.050	64.8
22.5	0.044	57.0
25.0	0.040	51.1
27.5	0.036	45.2
30.0	0.033	42.3
32.5	0.031	38.4
35.0	0.029	36.4

A plot of the minimum wavelength againt the reciprocal of the tube voltage is shown in Figure 16 in Appendix II. The gradient of the straight-line fit was 1.2459×10^{-6}, using Equation (24), the experimental value for Planck's constant is 6.64×10^{-34}. Using Equation (25), the value of error in this value is $\pm 1.38 \times 10^{-35}$, and so the experimental value of Planck's constant is $6.6(0.1) \times 10^{-34}$ Js. This is consistent with the accepted value of 6.63×10^{-34} Js[5]. Applying the partial derivative method in Equation (27) to the mean of the calculated value of h from each data point obtains a value of Planck's constant as $6.7(\pm 0.1) \times 10^{-34}$ J s, and so both methods appear consistent with eachother (and the accepted value) as expected.

DISCUSSION

Peak Splitting

Peak splitting is observed in the second order reflections of the stimulated emission peaks for the tungsten anode (see Figure 11), however it is not observed for the first-order reflections. This is because the effective resolution of the data increases with the order of reflection, n.

This is a consequence of the Bragg condition (Equation (8)), since taking the derivative with respect to λ yields:

$$\frac{d(sin(\theta))}{d\lambda} = \frac{n}{a} \tag{29}$$

And so the change in $sin(\theta)$ per unit change in wavelength, λ increases with the order of reflection, n. This rate of change is the resolution.

Errors

Both the experimental value of the lattice constant and the experimental value of Planck's constant were found to be consistent with accepted values.

For the calculation of the lattice constant the random error calculated from the statistical method was much less than the systematic error calculated from the partial derivative method. This is likely due to the fact that the statistical method assumes a large number of results which were not available due to the nature of the data obtained (there are few stimulated emission peaks and the data took a long time to collect so the range of tube voltages was also limited). In both cases, taking more measurements would improve the applicability of the statistical technique, and reduce the standard error, improving the results considerably.

For the data pertaining to the calculation of the lattice constant, errors in calibration could also a source of error, as this will disturb the required $\theta : 2\theta$ ratio in the geometry of the experimental set-up, which could cause reflections from unexpected planes. However, the observed results were consistent with what was expected and so it seems unlikely that this was a problem, as it would likely have a very disruptive effect.

Impurities in the Sodium Chloride crystal could also affect the results, although these are unlikely to be in significant enough quantities to produce a substantial change in the calculated lattice spacing. The concentrations of impurities could be investigated by various spectroscopic methods such as emission spectrometry.

For the calculation of Planck's constant it was difficult to judge the cut-off wavelength, since the count rate never drops to zero entirely (due to background radiation). In the calculation the first minimum was taken as the cut-off wavelength, however a more effective method might be to first measure the count rate of the background radiation and set this as the threshold count rate, though it is unlikely this change in method would significantly affect the analysis since there is a negligible difference between the wavelength of the first minimum and when it drops below a low value due to the sharp gradient of the cut-off.

CONCLUSIONS

The lattice spacing was found to be 565 ± 5 pm, this value is consistent with the accepted value of 564.02 pm.

The experimental value of Planck's constant was found to be $6.6(0.1) \times 10^{-34}$ Js. This is consistent with the accepted value of 6.63×10^{-34} Js.

To extend the investigation one could use a larger angular range and a higher tube voltage and current to attempt to detect K_α peak splitting for the greater order reflections for molybdenum anode, and use the same technique to thoroughly investigate the peak splitting from the tungsten anode, as the resolution increases at higher orders of refflection, although the intensity drops off rapidly.

[1] H. Young and R. Freedman, in *University Physics with Modern Physics* (Addison-Wesley, San Francisco, CA, 2007) pp. 1330–1331, 12th ed., ISBN 978-0-321-50121-9

[2] J. Als-Nielsen and D. McMorrow, in *Elements of Modern X-Ray Physics* (Wiley, New York, NY, 2001) p. 30, ISBN 0-471-49858-0

[3] M. Woolfson, in *An Introduction to X-Ray Crystallography* (Cambridge University Press, Cambridge, United Kingdom, 1997) p. 10, 2nd ed., ISBN 0-521-42359-7

[4] F. Fitzpatrick, in *Maxwell's Equations and the Principles of Electromagnetism* (Infinity Science Press LLC, Hingham, MA, 2008) pp. 124–131, ISBN 978-1-934015-20-9

[5] R. Serway, in *College Physics* (Brooks Cole, Pacific Grove, CA, 2005) p. 881, 7th ed., ISBN 978-0-534-99918-6

[6] *AN10 X-Ray Physics Experiment Manuscript*, `http://newton.ex.ac.uk/teaching/resources/au/phy2017/files/manuscripts/an10.pdf`

[7] G. Kaye and T. Laby, in *Tables of Physical and Chemical Constants* (Longhorn, 1986) Chap. 3.4.1 Characteristic X-ray Lines, 15th ed., ISBN 0-582-463548

[8] E. Prince, in *International Tables for Crystallography*, Vol. C (Kluwer Academic Publishers, Norwell, MA, 2004) Chap. 4.2, p. 191, ISBN 1-4020-1900-9

[9] S. Kasap and P. Capper, eds., in *Springer Handbook of Electronic and Photonic Materials* (Springer, New York, NY, 2006) p. 374, ISBN 978-0-387-26059-4

[10] N. Szwacki and T. Szwacka, in *Basic Elements of Crystallography* (Pan Stanford, Singapore, 2010) p. 135, ISBN 978-981-4241-59-5

Appendix I: Experimental results for determining the lattice spacing

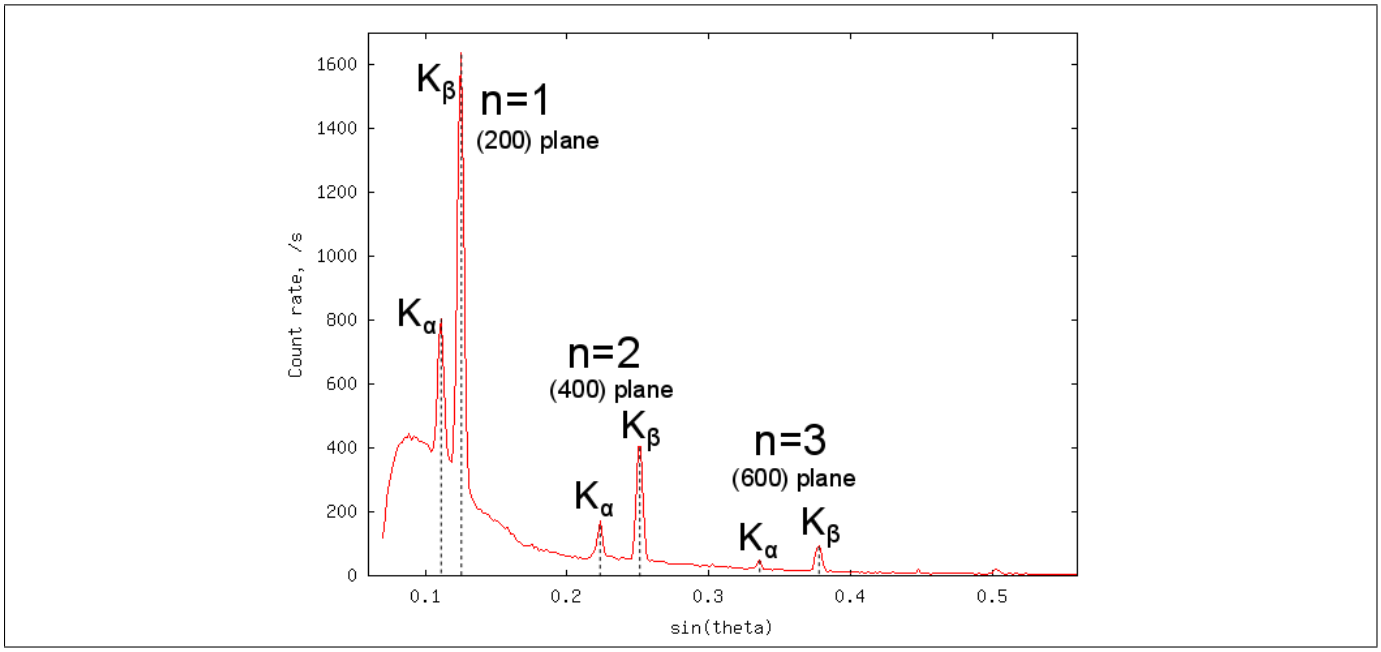

FIG. 10: A plot of the count rate against $sin(\theta)$ for the molybdenum anode. Three orders of reflection were observed, though no peak splitting was observable at this resolution.

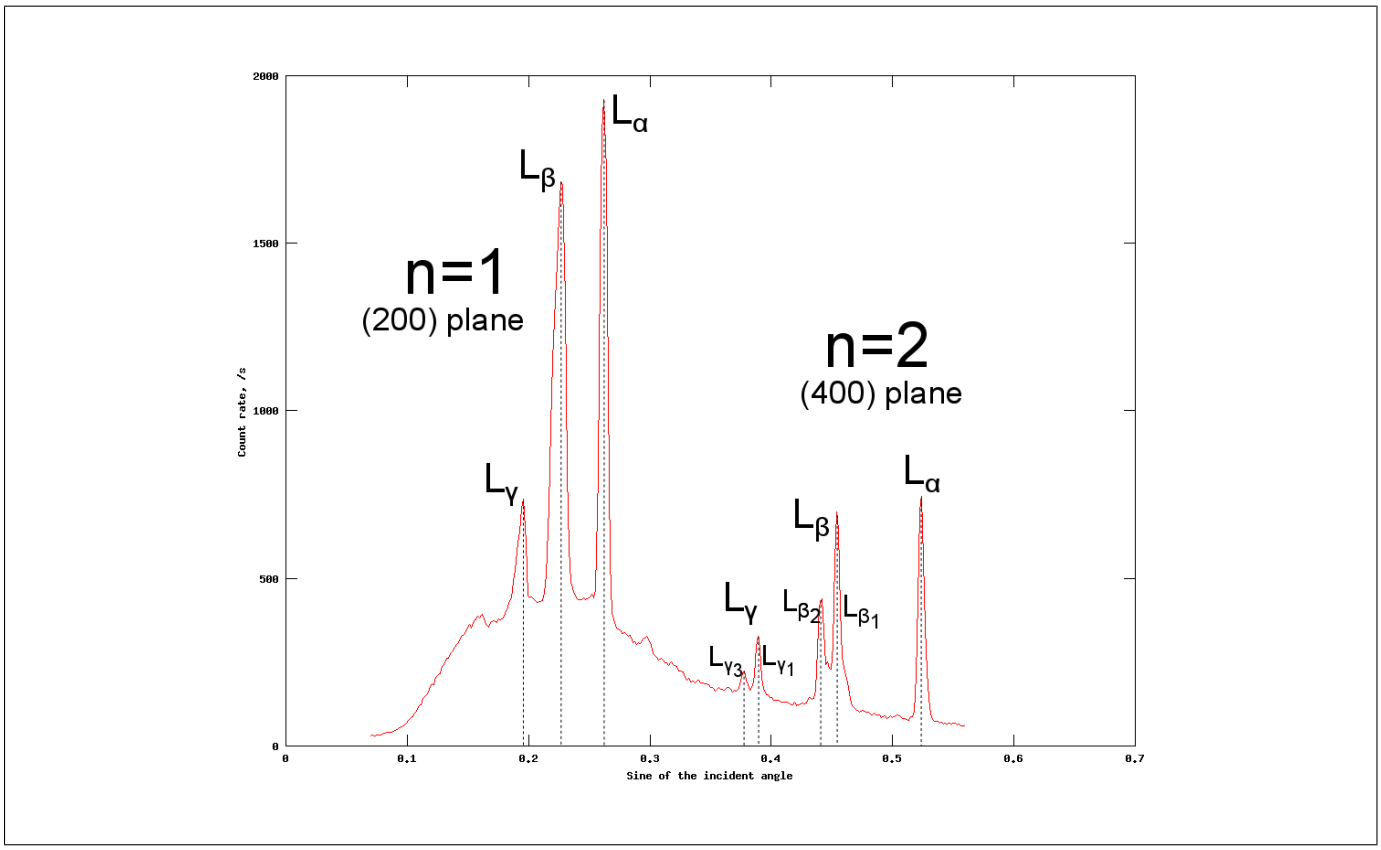

FIG. 11: A plot of the count rate against $sin(\theta)$ for the tungsten anode. Two orders of reflection were observed, and peak splitting was observed at the second order.

Appendix II: Experimental results for varying the tube voltage and current

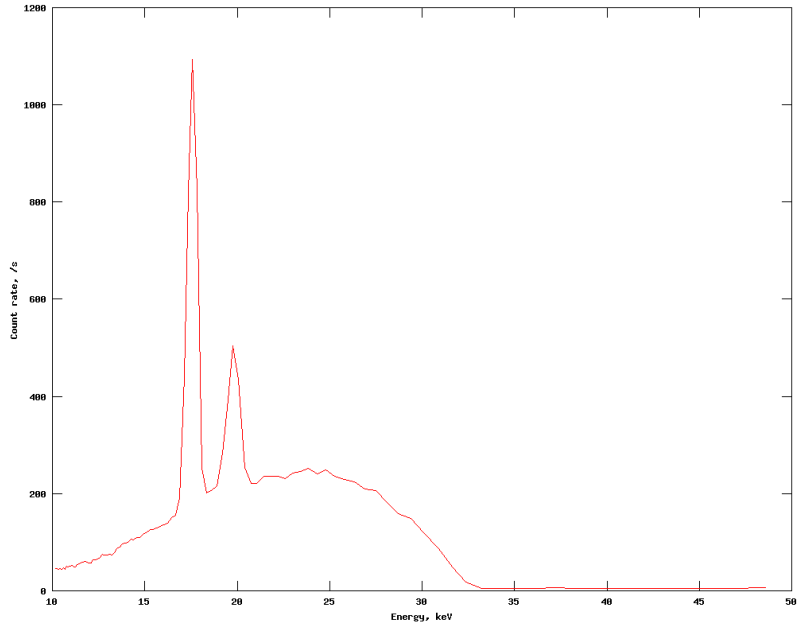

FIG. 12: A plot of the count rate against X-ray photon energy at a tube voltage of 35kV and a current of 1.0mA. This is the maximum current and maximum tube voltage.

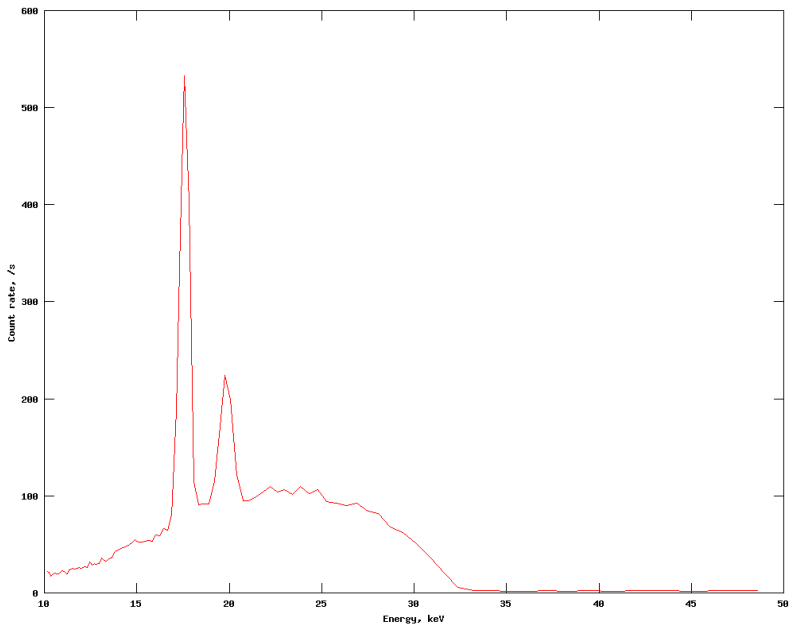

FIG. 13: A plot of the count rate against X-ray photon energy at a tube voltage of 35kV and a current of 0.4mA. This is the minimum current.

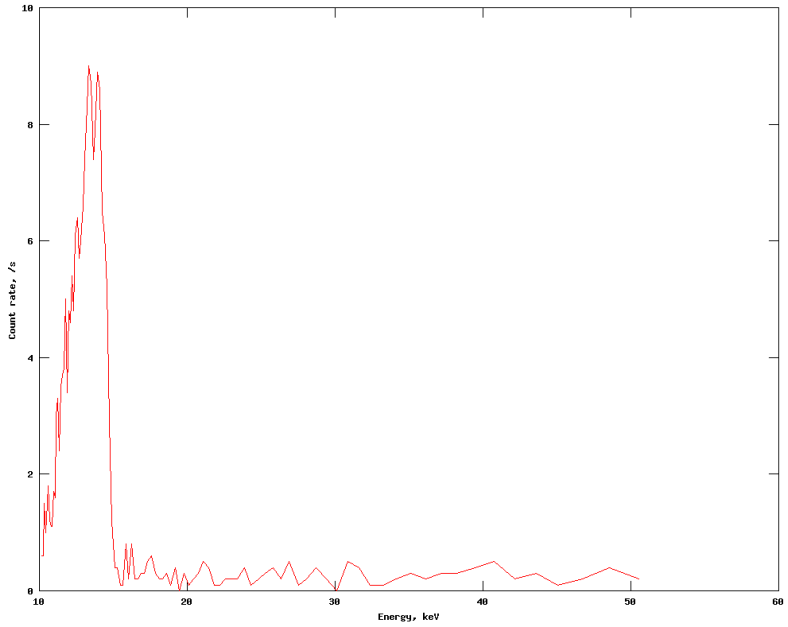

FIG. 14: A plot of the count rate against X-ray photon energy at a tube voltage of 15kV and a current of 1.0mA. This is the minimum tube voltage.

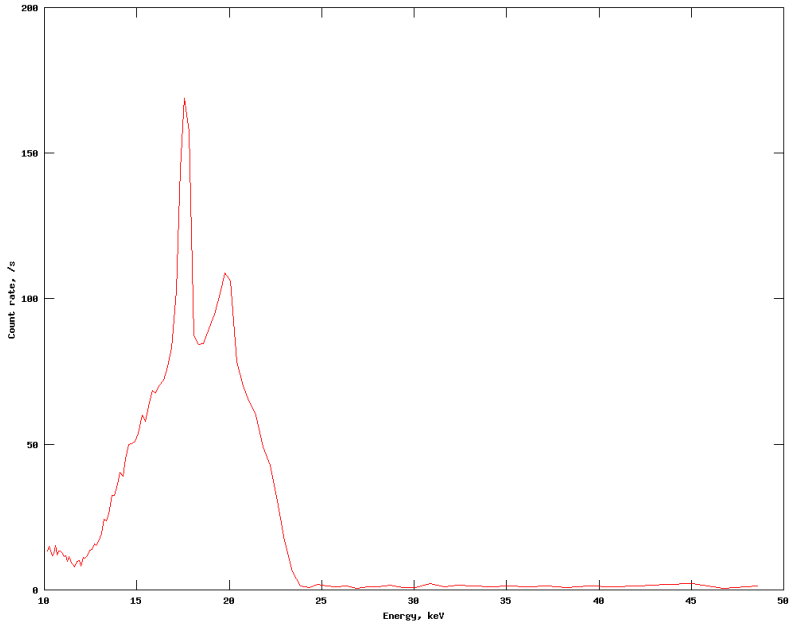

FIG. 15: A plot of the count rate against X-ray photon energy at a tube voltage of 25kV and a current of 1.0mA. This is the minimum tube voltage where the stimulated emission peaks are visible..

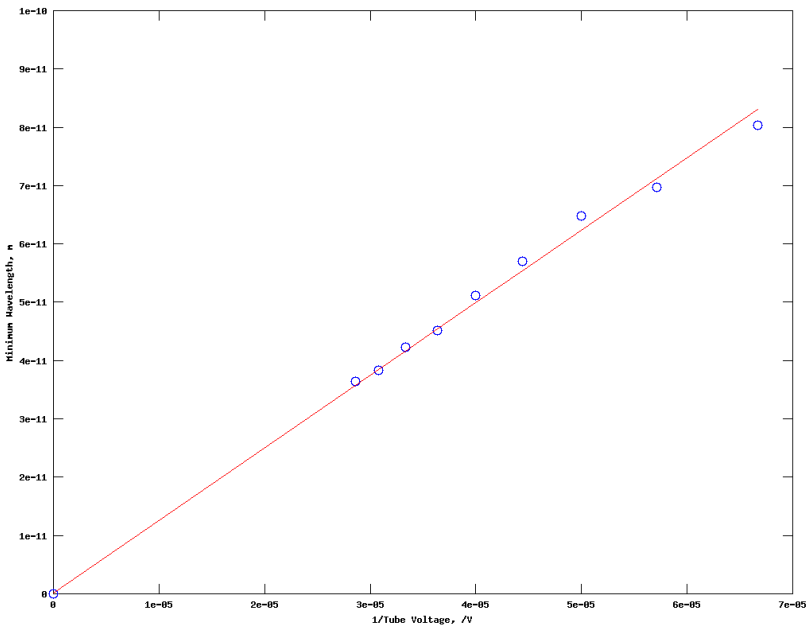

FIG. 16: A plot of the minimum wavelengths against the reciprocal of the tube voltage. The fit was forced through the origin as Equation (22) shows there should be no intercept. The equation for the straight line fit was $y = 1.2459 \times 10^{-6}x - 8.4396 \times 10^{-14}$.